PROCEEDINGS OF SCIENCE

The phase diagram at finite baryon and isospin densities at strong coupling

Wolfgang Unger[a,*]

[a] *Fakultät für Physik, Universität Bielefeld, Universitätstrasse 25, D33619 Bielefeld, Germany*

E-mail: wunger@physik.uni-bielefeld.de

The Hamiltonian formulation of lattice QCD with staggered fermions in the strong coupling limit can be extended to 2 flavors. It has no sign problem at non-zero baryon density and isospin densities and allows for Quantum Monte Carlo simulations. We have implemented a Quantum Monte Carlo algorithm to measure the baryon and isospin densities in the $\mu_B - \mu_I$ plane in the chiral limit. We also comment on the possibility to carry out corresponding simulations on a quantum computer.

The 40th International Symposium on Lattice Field Theory (Lattice 2023)
July 31st - August 4th, 2023
Fermi National Accelerator Laboratory

*Speaker

PoS(LATTICE2023)176

1. Introduction

The phase diagram of lattice QCD with staggered fermions in the strong coupling regime has been studied since decades for $N_f = 1$ in the $\mu_B - T$ plane, both via mean field theory [1–3] based on a $1/d$ expansion, and via Monte Carlo [4–6] based on the dual representation where the degrees of freedom are color singlets, such as mesons and baryons. This dual representation is obtained by integrating out the gauge fields and the Grassmann variables analytically, resulting in a much milder finite density sign problem, as the sign only depends on the the geometry of baryonic world-lines. This effective theory of lattice QCD can be very efficiently simulated by the worm algorithm [6] and has been extended via the strong coupling expansion to non-zero values of the inverse gauge coupling $\beta = \frac{2N_c}{g^2}$ [7].
The drawback of the dual representation is that the sign problem is gradually re-introduced as the lattice gets finer, hence the continuum limit is out of reach. The phase diagram in the strong coupling regime features a critical endpoint at finite quark mass (tricritical in the chiral limit [8]), which for moderate quark masses is located at values much larger than $\mu_{B,c}/T_c > 3$ [9]. Whether the chiral critical point still exists in the continuum limit is still unknown.

To vary the temperature continuously for $\beta = 0$, it is necessary to use anisotropic lattices, with γ the bare anisotropy and $a/a_t \equiv \xi(\gamma)$, the physical anisotropy, such that the temperature in lattice units is $aT = \xi/N_\tau$. We make use of the continuous Euclidean time limit, discussed in detail in [10, 11], where $a_t \to 0$ and $N_t \to \infty$ are taken simultaneously, while the temperature remains fixed. It is then possible to map the corresponding partition function to a Quantum Hamiltonian formulation of lattice QCD, where the Euclidean time extend corresponds to the inverse of the temperature $\mathcal{T}$. This is computationally advantageous (using Quantum Monte Carlo instead the discrete time Worm algorithm) and the Hamiltonian can also be used to construct a set of quantum circuits that potentially can run on a quantum computer [12].

In this proceedings we report on the progress on the strong coupling phase diagram for $N_f = 2$: the dual formulation is only sign-problem free in the continuous Euclidean time limit. Again, in this limit, a quantum Hamiltonian formulation can be established, and simulated via Quantum Monte Carlo, which has been outlined in [13]. In this study, we perform simulations at both non-zero baryon and isospin density, and preliminary results on the phase diagram in the $\mu_B - \mu_I - T$ are presented.

2. Hamiltonian formulation in the strong coupling limit for $N_f = 2$

While it is possible to derive a Hamiltonian formulation for gauge group SU(3) for any number of flavors, for definiteness we will here restrict to the formulation for $N_f = 2$ in the chiral limit. It should be noted that the number of hadronic states quickly grows with the number of flavors, the dimension d of the local Hilbert space $\mathbb{H}_\mathfrak{h}$ (=states per spatial site) is $d = 6$ for $N_f = 1$, $d = 92$ for $N_f = 2$ and $d = 2074$ for $N_f = 3$. The full Hilbert space has thus dimension $D = d^\Omega$ with $\Omega = N_s^3$ the spatial lattice volume. To refine the 92 states for $N_f = 2$ further, the one-link integral in the presence of the 3×3-dimensional quark matrices M, $M^\dagger$ (summed over flavors f, g) has to be

computed:

$$\mathcal{J}(\mathcal{M},\mathcal{M}^\dagger) = \int\limits_{\mathrm{SU}(3)} dU e^{\mathrm{tr}[U\mathcal{M}^\dagger + U^\dagger \mathcal{M}]} = \sum_{B=-2}^{2} \sum_{n_1,n_2,n_3} C_{B,n_1,n_2,n_3} \frac{E^B}{|B|!} \prod_{i=1}^{3} \frac{X_i^{n_i}}{n_i!}, \quad E = \begin{cases} \det \mathcal{M} & B > 0 \\ 1 & B = 0 \\ \det \mathcal{M}^\dagger & B < 0 \end{cases}$$

$$(\mathcal{M})_{ij} = \bar{\chi}_i^f(x)\chi_i^f(y), \quad (\mathcal{M}^\dagger)_{kl} = \chi_k^g(y)\bar{\chi}_l^g(x),$$
$$X_1 = M_{\pi_U} + M_{\pi_D} + M_{\pi^+} + M_{\pi^-}, \quad D_2 = M_{\pi_U}M_{\pi_D} + M_{\pi^+}M_{\pi^-} - M^{(2)}_{\pi^+\pi^-,UD} - M^{(2)}_{UD,\pi^+\pi^-}$$
$$X_2 = X_1^2 - D_2, \quad X_3 = X_1^3 - 2X_1 D_2,$$
$$\det \mathcal{M} = B_{uuu} + B_{uud} + B_{udd} + B_{ddd}, \quad \det \mathcal{M}^\dagger = \bar{B}_{uuu} + \bar{B}_{uud} + \bar{B}_{udd} + \bar{B}_{ddd} \tag{1}$$

where the invariants X_i and coefficients C_{B,n_1,n_2,n_3} were discussed in [13]. The M_{π_i} are meson hoppings (with $\pi_1 = \pi_U$, $\pi_2 = \pi_D$, $\pi_3 = \pi_{\pi^+}$, $\pi_4 = \pi^-$) between nearest neighbor sites $\langle x, y\rangle$, the B_{fgh} are baryons hopping from x to y and $\bar{B}_{fgh}$ anti-baryons hopping from y to x. After Grassmann integration, negative weights occur within the invariant X_2, X_3 due to non-trivial Wick contractions from D_2. However, in the continuous time limit, only single meson exchange survives and in particular the two-meson hoppings $M^{(2)}_{\pi^+\pi^-,UD}$, $M^{(2)}_{UD,\pi^+\pi^-}$ can only appear in temporal direction. After diagonalization of the transfer matrix only 92 distinct hadronic states survive, which all have positive weight. Few of these states with the same quark content are two-fold degenerated, e.g. :

$$|\pi_1^2\rangle = \sqrt{3}|M_{\pi_U}M_{\pi_D}\rangle + |M^{(2)}_{UD,\pi^+\pi^-}\rangle, \qquad |\pi_2^2\rangle = \sqrt{3}|M_{\pi^+}M_{\pi^-}\rangle + |M^{(2)}_{\pi^+\pi^-,UD}\rangle \tag{2}$$

The 92 quantum states are classified by baryon number B, isospin number I and mesons occupation number $\mathfrak{m}$. Since we are restricted to the chiral limit, a conservation law for each of the pion currents of π_U, π_D, π_+, π_- holds. The role of spatial dimers at a bond location $\langle x, y\rangle$ is to transfer pion charge from one site x to site y. Due to the even-odd ordering for staggered fermions, such dimers can be consistently oriented from an emission site x to an absorption site y. As a consequence, if a occupation number $\mathfrak{m}_{\pi_i}(x)$ is raised/lowered by a spatial dimer, then at the site connected by the spatial meson hopping the meson occupation number $\mathfrak{m}_{\pi_i}(y)$ is lowered/raised. With those interactions derived from a high temperature series, the resulting partition sum can be expressed in terms of a Hamiltonian that is composed of mesonic annihilation and creation operators $\hat{J}^\pm_Q$:

$$Z_{\mathrm{CT}}(\mathcal{T},\mu_{\mathcal{B}},\mu_I,\Omega) = \mathrm{Tr}_{\mathfrak{h}^\Omega}\left[e^{(\hat{\mathcal{H}}+\hat{\mathcal{N}}_B\mu_{\mathcal{B}}+\hat{\mathcal{N}}_I\mu_I)/\mathcal{T}}\right] \qquad \mathfrak{h} \in \mathbb{H}_{\mathfrak{h}}$$
$$\hat{\mathcal{H}} = \frac{1}{2}\sum_{\langle\vec{x},\vec{y}\rangle}\sum_{\pi_i\in\{\pi^+,\pi^-,\pi_U,\pi_D\}}\left(\hat{J}^+_{\pi_i,\vec{x}}\hat{J}^-_{\pi_i,\vec{y}} + \hat{J}^-_{\pi_i,\vec{x}}\hat{J}^+_{\pi_i,\vec{y}}\right)$$
$$\hat{\mathcal{N}}_B = \mathrm{diag}(-2,-1,\ldots 1,2), \qquad \hat{\mathcal{N}}_I = \mathrm{diag}\left(0,-\frac{3}{2},\ldots\frac{3}{2},0\right) \tag{3}$$

where the matrices per spatial site, $\hat{J}^+_{\pi_i}$, $\hat{J}^-_{\pi_i}$, $\hat{\mathcal{N}}_B$ and $\hat{\mathcal{N}}_I$ are 92×92 - dimensional and the tensor product over all spatial sites Ω is implied and $\mathbb{H}_{\mathfrak{h}}$ is the 92-dimensional local Hilbert space. For the transition $\mathfrak{h}_1 \mapsto \mathfrak{h}_2$, the matrix elements $\langle\mathfrak{h}_1|\hat{J}^\pm_{\pi_i}|\mathfrak{h}_2\rangle$ are determined from Grassmann integration and diagonalization, only those matrix elements are non-zero which are consistent with current conservation of all π_i.

Since meson occupation numbers are not just bounded from below, but also from above due to the Grassmannian nature of the underlying quarks, they fulfill an algebra that exhibits a particle-hole symmetry. The matrices $\hat{J}^{\pm}_{\pi_i}$ hence span a $\frac{3}{2}(2-|B|)$-dimensional representation of a SU(2) Lie algebra (for details see [13]). The representation for $\hat{J}^{\pm}_{\pi_U}$ and $\hat{J}^{\pm}_{\pi_D}$ is a direct product representation, likewise $\hat{J}^{\pm}_{\pi^+}$ and $\hat{J}^{\pm}_{\pi^-}$, and they fulfill the following identities:

$$[\hat{J}^{+}_{\pi_i}, \hat{J}^{-}_{\pi_i}] = \frac{2}{N_c}\hat{J}^{(3)}_{\pi_i}, \qquad [\hat{J}^{+}_{\pi_i}, \hat{J}^{-}_{\pi_j}] = 0 \quad \text{for} \quad i \neq j. \tag{4}$$

We label all 92 hadronic states of the local Hilbert space by their quark content in lexicographical order: first ordered by B, I and $\mathfrak{m}$ and then by the sequence of occupations in $\bar{u}$, u, $\bar{d}$, d. However, the quark content is not sufficient to distinguish those 6 states that are two-fold degenerate: here we introduce an additional index $q \in \{0, 1\}$.

3. Quantum Monte Carlo Simulation and Results on the Phase Diagram

The $N_f = 2$ QMC algorithm is an extension of the $N_f = 1$ QMC and is also realized as a continuous time version of the worm algorithm for strong coupling LQCD [10] and has been described in [13]. The essential part is that for each of the the possible states $\{\pi_U, \pi_D, \pi_+, \pi_-\}$, chosen randomly, $\hat{J}^{+}_{\pi_i}$, $\hat{J}^{-}_{\pi_i}$ will be fixed during worm evolution until the worm closes. The worm evolution in continuous Euclidean time is essentially a Poisson process. The baryon and isospin densities can be measured on each configuration after each worm update. Also the chiral and pion susceptibilities can be obtained from the integrated 2-point correlation functions measured during worm evolution as so-called improved estimators.

The thermodynamic observables in the chiral limit we investigate are: the baryon density, $\langle n_B \rangle = \frac{\mathcal{T}}{\Omega}\frac{\partial \ln Z}{\partial \mu_B}$, which signals the nuclear transition at $\langle n_B \rangle \simeq 1$ for $T < 1.0$, and is its Pauli saturation at $\langle n_B \rangle = 2$; the isospin density $\langle n_I \rangle = \frac{\mathcal{T}}{\Omega}\frac{\partial \ln Z}{\partial \mu_I}$, which is only non-zero in the nuclear transition region, and is expected to vanish in the chirally broken and Pauli saturated phase (this is a lattice artifact at strong coupling that should not hold in the continuum limit); the interaction energy: the density of spatial pion exchange $\langle \sum_{\pi_i} M^{\text{spat}}_{\pi_i} \rangle / \Omega$, which is a measure for chiral symmetry breaking.

At non-zero isopsin chemical potential μ_I, it is expected from mean field theory [3] that there are two chiral transition at zero temperature: $\mu^{(u)}_{B,c}$ where the chiral condensate $\langle \bar{u}u \rangle$ vanishes, and $\mu^{(d)}_{B,c}$ where $\langle \bar{d}d \rangle$ vanishes, and $\mu^{(d)}_{B,c} > \mu^{(u)}_{B,c}$ as the $\mu_I > 0$ favors up quarks over down quarks.

From a scan in the parameters μ_B, μ_I and $\mathcal{T}$, the observables could be measured in various planes as shown in Fig. 1. They indicate phase transitions between a vacuum and a finite baryon/isopin density phase, and a chirally broken phase. A preliminary phase diagram that summarizes the location of the transitions could be established ans is shown in Fig. 2. We find that the nuclear transition μ^c_B depends strongly on μ_I, but weakly on temperature $\mathcal{T}$. The location of the critical endpoint is not yet established: all data based on 8^3 volume, the order of the transition requires finite size scaling using isospin and baryon susceptibilities, which we will carry out after

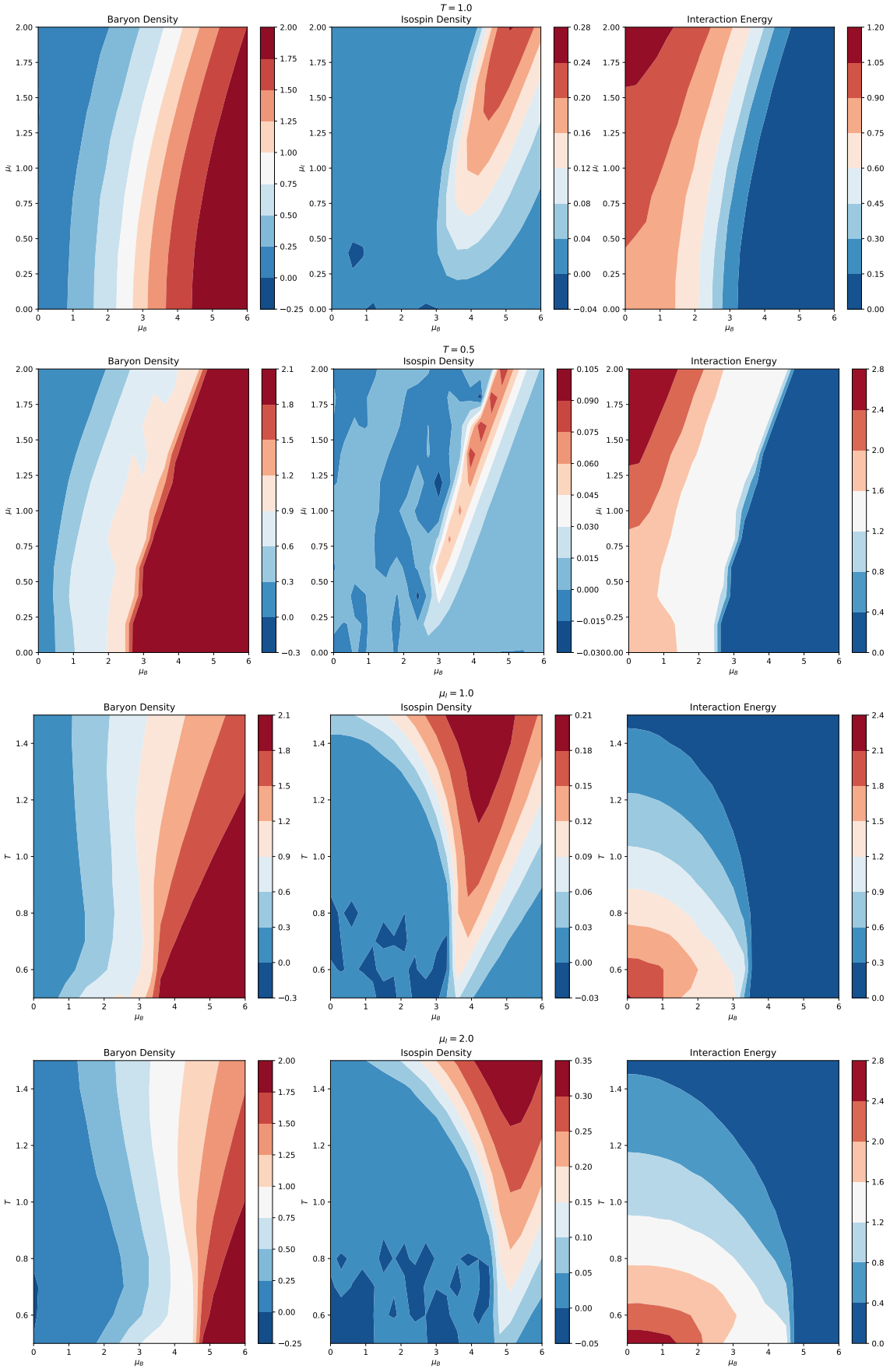

μ_B-T-plane for various isospin chemical potential μ_I:

Figure 1: Observables: baryon density (*left*), isospin density (*center*), interaction energy (*right*) in the $\mu_B - \mu_I$-plane for temperatures $T = 1.0$ (*first row*) and $T = 0.5$ (*second row*), and in the $\mu_B - T$ plane for isospin chemical potential $\mu_I = 1.0$ (*third row*) and $\mu_I = 2.0$ (*last row*).

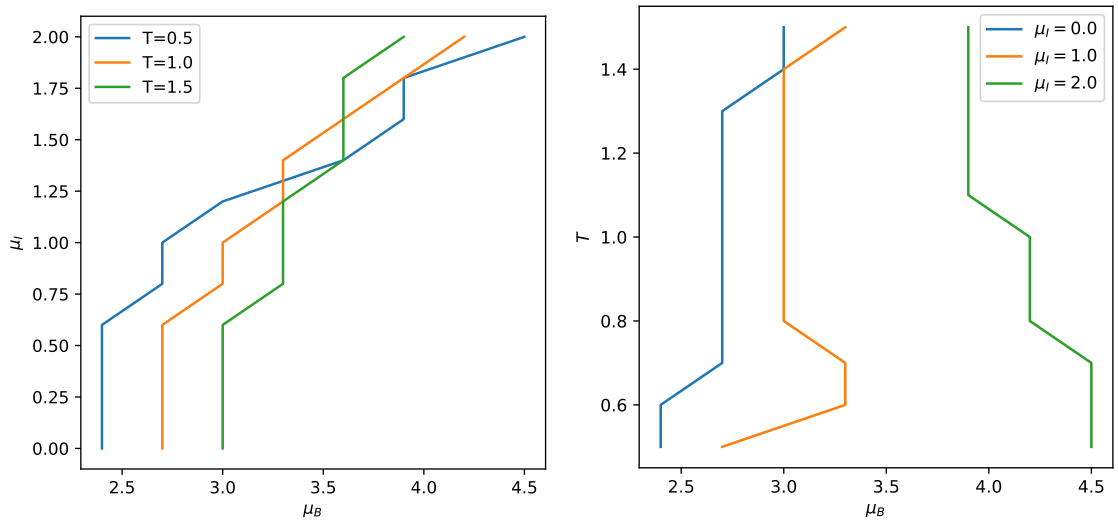

Figure 2: Preliminary result for the scans in μ_B, μ_I and T. *Left:* $\mu_B - \mu_I$ plane for various temperatures. *Right:* $\mu_B - T$ plane for various isospin chemical potential.

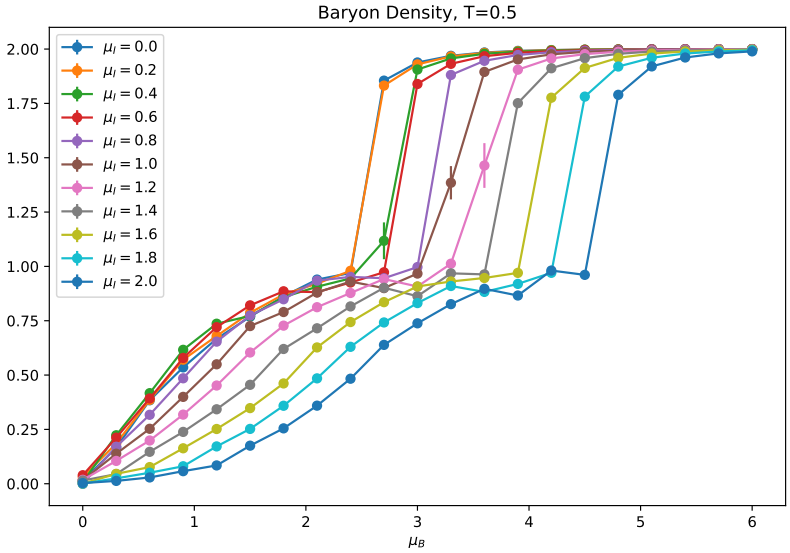

Figure 3: Baryon density for the lowest temperature obtained so far, $\mathcal{T} = 0.5$, indicating a strong first order transition that increases with isospin chemical potential. There is an indication for plateau of the baryon density $\langle n_B \rangle = 1$, which might be more pronounced at lower temperatures.

further improvements on performance are implemented. The lowest temperature obtained so far is $aT = 0.5$, which features a first order nuclear transition. Although the simulations do not yet show a plateau at $\langle n_B \rangle = 1$, two two regimes are present in Fig. 3 that possibly indicated two transitions at lower temperatures, which are computationally expensive.

4. Summary and Outlook

We have used the Hamiltonian formulation of strong coupling lattice QCD for $N_f = 2$ staggered fermions to perform continuous time quantum Monte Carlo simulations that have no sign problem, even for both non-zero baryon and isospin chemical potential. We mapped out the enlarged phase diagram in the $\mu_B - \mu_I - T$-space in the chiral limit, based on the baryon and isospin densities. All results have been obtained on spatial lattice 8^3 and continuous time. The finite size scaling analysis to determine the order of the transition in the thermodynamic limit will be presented in a forthcoming publication. We will also address pion condensation and the chiral transitions, and determine the nuclear interactions, which are purely entropic for $N_f = 1$, but allow for pion exchange between nucleons for $N_f = 2$. It should be noted that these findings are qualitatively in agreement with $Nf = 2$ Mean field theory at strong coupling, but not in agreement with expectations in the continuum limit for zero μ_B and non-zero μ_I [14]. However, the strong coupling limit gives further insights in the nature of the phases.

Recently, the $N_f = 1$ quantum Hamiltonian has been mapped on quantum circuits [12]: since the degrees of freedom are already discrete, it can be easily qubitzed. Gauge group SU(3) only required three qubits. As Gauss's law is fulfilled implicitly due to the occupation number basis, it can be readily applied to 3 spatial dimensions. For $N_f = 2$ the mesonic sector U(3) requires 6 qubits per lattice site, and at most 6 additional qubits per site when baryons are included. The quantum gates corresponding to the set of mutually commuting families still need to be worked out. For the future, we also plan to extend the Hamiltonian framework to address finite quark masses, and to include the gauge corrections to the strong coupling limit. It is not yet guaranteed that these extensions are sign-problem free, but it is in any case much milder than on a lattice with discrete time.

The author gratefully acknowledge the funding of this project by computing time provided by the Paderborn Center for Parallel Computing (PC^2). This work is supported by the Deutsche Forschungsgemeinschaft (DFG) through the CRC-TR 211 'Strong-interaction matter under extreme conditions'– project number 315477589 – TRR 211.

References

[1] N. Kawamoto and J. Smit. Effective Lagrangian and Dynamical Symmetry Breaking in Strongly Coupled Lattice QCD. *Nucl. Phys.*, B192:100, 1981. [,556(1981)].

[2] Neven Bilic, Frithjof Karsch, and Krzysztof Redlich. Flavor dependence of the chiral phase transition in strong coupling QCD. *Phys. Rev.*, D45:3228–3236, 1992.

[3] Yusuke Nishida. Phase structures of strong coupling lattice QCD with finite baryon and isospin density. *Phys. Rev.*, D69:094501, 2004.

[4] Pietro Rossi and Ulli Wolff. Lattice QCD With Fermions at Strong Coupling: A Dimer System. *Nucl. Phys.*, B248:105–122, 1984.

[5] F. Karsch and K. H. Mutter. Strong Coupling QCD at Finite Baryon Number Density. *Nucl. Phys.*, B313:541–559, 1989.

[6] Ph. de Forcrand and M. Fromm. Nuclear Physics from lattice QCD at strong coupling. *Phys. Rev. Lett.*, 104:112005, 2010.

[7] G. Gagliardi and W. Unger. New dual representation for staggered lattice QCD. *Phys. Rev. D*, 101(3):034509, 2020.

[8] Ph. de Forcrand, J. Langelage, O. Philipsen, and W. Unger. Lattice QCD Phase Diagram In and Away from the Strong Coupling Limit. *Phys. Rev. Lett.*, 113(15):152002, 2014.

[9] J. Kim, P. Pattanaik and W. Unger, 'Nuclear liquid-gas transition in the strong coupling regime of lattice QCD," Phys. Rev. D **107** (2023) no.9, 094514 [arXiv:2303.01467 [hep-lat]].

[10] M. Klegrewe and W. Unger. Strong Coupling Lattice QCD in the Continuous Time Limit. *Phys. Rev. D*, 102(3):034505, 2020.

[11] Ph. de Forcrand, W. Unger, and H. Vairinhos. Strong-Coupling Lattice QCD on Anisotropic Lattices. *Phys. Rev.*, D97(3):034512, 2018.

[12] M. Fromm, O. Philipsen, W. Unger and C. Winterowd, "Quantum Gate Sets for Lattice QCD in the strong coupling limit: $N_f = 1$," [arXiv:2308.03196 [hep-lat]].

[13] W. Unger and P. Pattanaik, "Towards Quantum Monte Carlo Simulations at non-zero Baryon and Isospin Density in the Strong Coupling Regime," PoS **LATTICE2022** (2023), 162 [arXiv:2212.11328 [hep-lat]].

[14] B. B. Brandt, G. Endrodi and S. Schmalzbauer, "QCD phase diagram for nonzero isospin-asymmetry," Phys. Rev. D **97** (2018) no.5, 054514 doi:10.1103/PhysRevD.97.054514 [arXiv:1712.08190 [hep-lat]].